Supporting Information:

A Cell-Targeted, Size-Photocontrollable, Nuclear-Uptake Nanodrug Delivery System for Drug-Resistant Cancer Therapy

Liping Qiu[†], Tao Chen[†,‡], Ismail öçsoy[‡], Emir Yasun[‡], Cuichen Wu[‡], Guizhi Zhu[†,‡], Mingxu You[†,‡], Da Han[‡], Jianhui Jiang[†], Ruqin Yu[†] and Weihong Tan[†,‡,*]

[†] Molecular Science and Biomedicine Laboratory, State Key Laboratory for Chemo/Bio-Sensing and Chemometrics, College of Chemistry and Chemical Engineering, College of Biology, and Collaborative Research Center of Molecular Engineering for Theranostics, Hunan University, Changsha 410082, China

[‡]Center for Research at Bio/Nano Interface, Department of Chemistry and Department of Physiology and Functional Genomics, Health Cancer Center, UF Genetics Institute and McKnight Brain Institute, University of Florida, Gainesville, Florida 32611-7200, United States

[*]To whom correspondence should be addressed: E-mail: tan@chem.ufl.edu; Tel/Fax: +1 352 846 2410

Table S1. DNA Sequences Designed in This Work.

Note	Sequence (5'→ 3')
Drug loading/anchoring strand (DAS)	HS-ttt CGT CGT CGT CGT CGT CGT ttttttttt TTGTGGTGGTGGTGG(TAMR)
Drug-loading cDNA	ACG ACG ACG ACG ACG ACG
Capture Strand (CS)	HS-ttttttttt CCA CCA CCA CCA CAA
Sgc8	(FITC/Cy5)ATCTAACTGCTGCGCCGCCGGGAAAATACTGTACGGTTAGAttttttttt-HS
KK1B10	(FITC)ACAGCAGATCAGTCTATCTTCTCCTGATGGGTTCCTATTTATAGGTGAAGC TGT ttttttttt-HS

Note: "HS" represents the thiol group. The "TAMRA", "FITC" and "Cy5" in the brackets indicate that the corresponding sequence was modified with one or none of these fluorophores, according to experimental requirements.

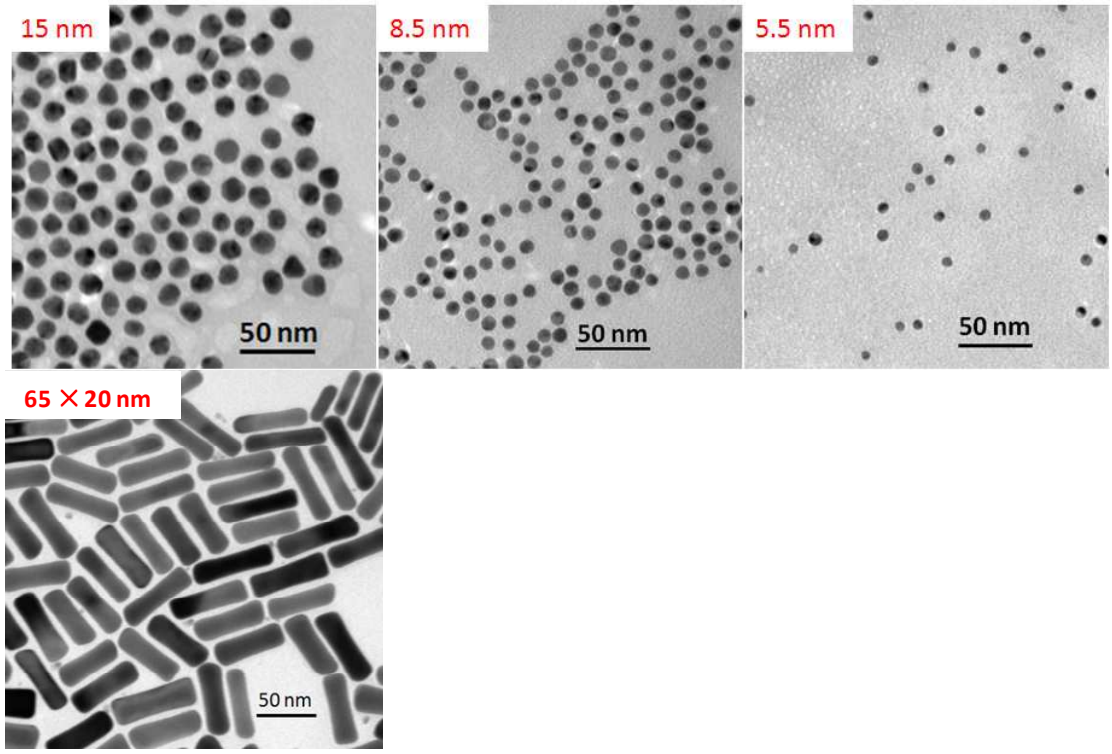

Figure S1. TEM images of Gold Nanoparticles (NPs) of different sizes and Gold-silver nanorods (NRs).

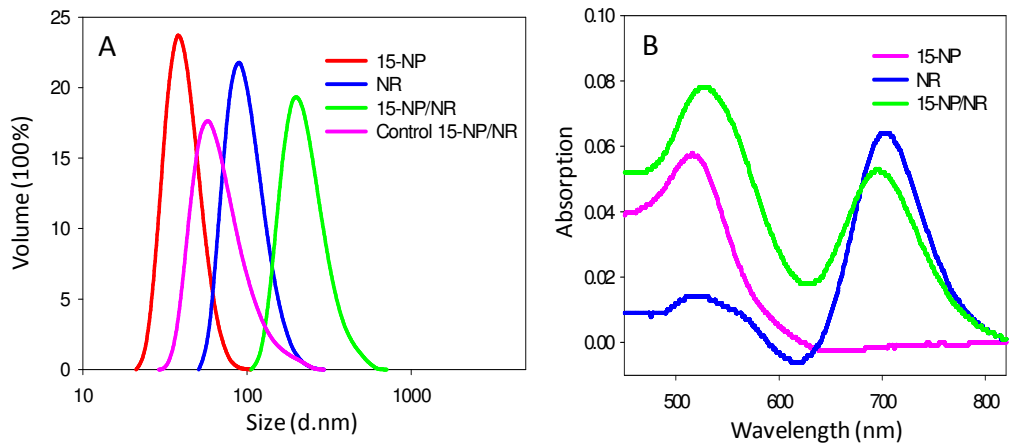

Figure S2. Characterization of different nanomaterials. (A) Dynamic light scattering (DLS) spectra and (B) UV-vis spectra of 15-NP, NR, and 15-NP/NR.

To further understand the self-assembly process, DLS and UV-vis absorption spectroscopy measurements were performed. The average hydrodynamic diameter of the 15-NP, NR, and 15-NP/NR were 37.8±1.3, 91.3±2.1, and 190.1±3.6 nm, respectively (Figure S2A), corresponding well with the values obtained from TEM. The increased size of the 15-NP/NR nanostructure further confirms the successful assembly of NPs and NRs. To demonstrate that the assembly between NPs and NRs arises from DNA hybridization, the CS was replaced with a thiolated random DNA sequence during the NR modification step. A relatively small average size (58.8 nm) resulting from the mixture of 15-NPs and NRs was detected by DLS, indicating that assembly did not occur. In the UV-vis spectra, the longitudinal plasmon band of the 15-NP/NR nanoassembly underwent a blue shift of 7 nm compared with the original NRs, while a clear red shift of 9 nm occurred in the transverse plasmon band (Figure S2B). These changes in surface plasmon resonance (SPR) may be attributed to the "flattening" of the NRs via side attachment of NPs, as indicated in a previous report.[5]

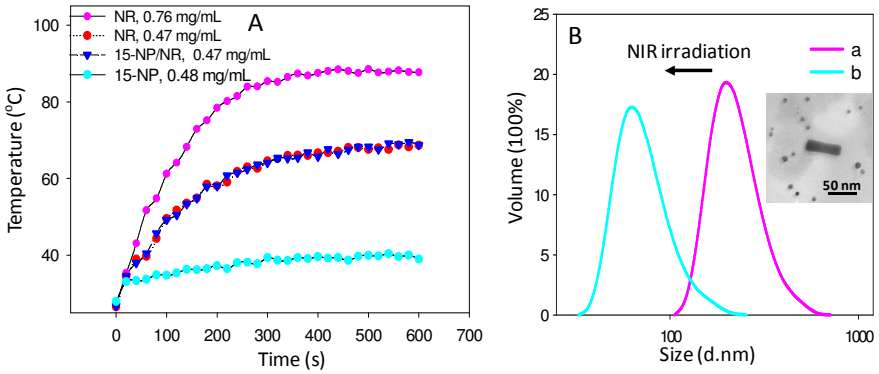

Figure S3. (A) Temperature-time curves of the medium with different nanomaterials at a specific concentration with NIR laser irradiation (808 nm, 600 mW/cm^2). (B) DLS spectra of 15-NP/NR before (curve a) and after (curve b) NIR irradiation; inset: TEM of 15-NP/NR after NIR irradiation.

After synthesizing and characterizing these nanoassemblies, we next investigated their NIR-response capability and drug-carrying potential. Their photothermal conversion capability was evaluated by monitoring the medium temperature with a tiny thermometer probe. Upon NIR irradiation, the medium temperature of NRs (0.76 mg/mL) increased significantly and reached ~85 ^{o}C at 300 s, while that of 15-NPs (0.48 mg/mL) changed at a much slower rate (Figure S3A). It should be noted that the slight temperature jump in the NP solution at the beginning resulted from the heat produced by the working thermometer probe, not the NP. The attachment of 15-NPs on the NR's side face had no influence on its photothermal behavior, as verified by the matching pattern of NRs and 15-NP/NRs in the time-dependent temperature plots when the NR concentration in both samples was 0.47 mg/mL. Of note, unlike the bulk medium, the temperature around the NR surface should jump rapidly upon laser irradiation irrespective of NR concentration, causing rapid denaturation of the CS/DAS duplex. The NIR-activated release of NPs from NRs was demonstrated by DLS and TEM. As shown in Figure S3B, the DLS profile of

the 15-NP/NR nanocomplexes shifts back to smaller average diameter after exposure to the laser, corresponding well with the random distribution between NPs and NRs from TEM, revealing dissociation of the nanoassemblies.

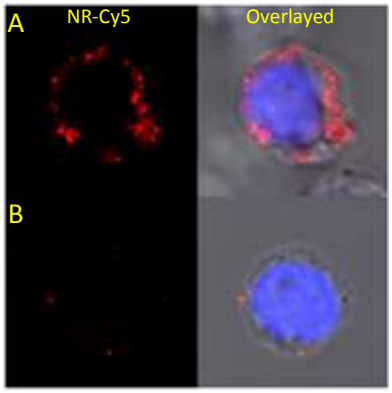

Figure S4. CLSM images of CEM cells (A) and Ramos cells (B) treated with NR-Sgc8s. The red fluorescence arises from the Cy5 fluorophore labeled on Sgc8, which was conjugated on the NR ends. The blue fluorescence is the result of nuclear staining (Hoechst 33342).

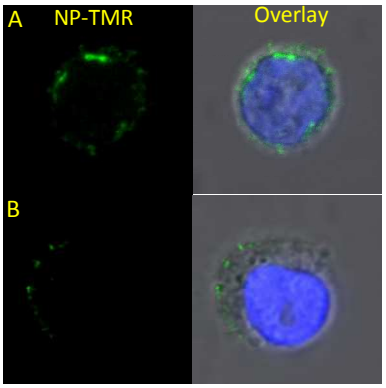

Figure S5. CLSM images of CEM cells incubated with 15-NPs and 15-NP/NR-Sgc8s (15-NPs: 0.062 mg/mL) at 37 ^{o}C for 6 h. The green fluorescence arises from the TAMRA fluorophore labeled on DAS, which was modified on NPs. The blue fluorescence is the result of nuclear staining (Hoechst 33342).

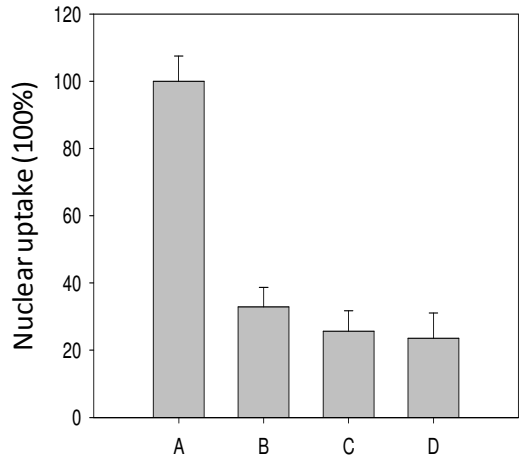

Figure S6. ICP-AES assay of NPs accumulated in the nuclei of CEM cells with treatment of 8.5-NP/NR-Sgc8 with (A) or without (B) NIR irradiation, or with treatment of 15-NP/NR-Sgc8 with (C) or without (D) NIR irradiation. The Au element signal intensity of sample A is defined as 100%, while that of other samples is the normalized value.

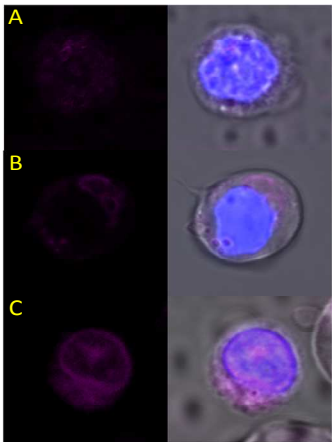

Figure S7. CLSM image of CEM cells after treatment with 8.5-NP-Dox/NR-Sgc8s with (A) or without (B) NIR irradiation, and treatment with free Dox (C). The pink fluorescence arises from Dox. The blue fluorescence is the result of nuclear staining (Hoechst 33342).

To perform these CLSM measurements, CEM cells were incubated with 8.5-NP-Dox/NR-Sgc8s at 37 ^{o}C for 6 h, washed three times, irradiated with (A) or without (B) NIR laser, incubated at 37 ^{o}C with 5% CO_2 for another 22 h, and then monitored with CLSM. As a control, CEM cells were incubated with free Dox at 37 ^{o}C for 6 h, washed three times, and incubated at 37 ^{o}C with 5% CO_2 for another 22 h.

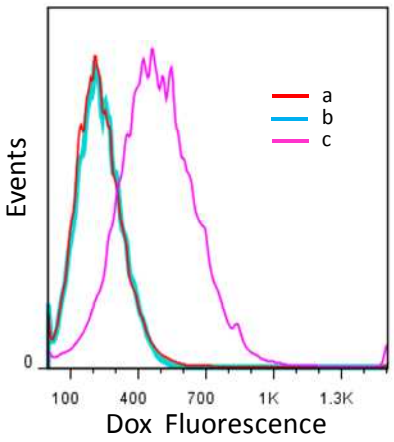

Figure S8. The influence of the laser irradiation (808 nm, 600 mW/cm^2, 10 min) on the stability of the NP-Dox complex. CEM cells were incubated with 8.5-NP-Dox/NR-Sgc8s and then irradiated with the laser. Flow cytometry were performed to record the Dox signal at different stages: before (curve a) and right after (curve b) laser irradiation, or 22 h later after laser irradiation (curve c).

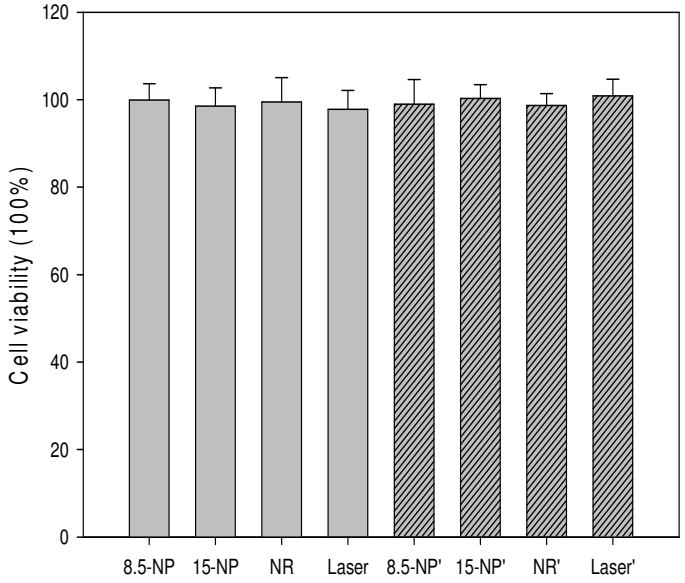

Figure S9. Cytotoxicity assay of CEM cells (gray column) and Ramos cells (shaded column) with treatments of 8.5-NPs (0.32 mg/mL), 15-NPs (0.32 mg/mL), and NRs (0.32 mg/mL) at 37 ^{o}C for 2 h, or irradiated with NIR laser for 10 min.

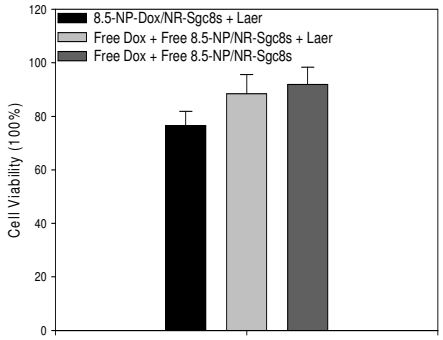

Figure S10. Cytotoxicity assay of CEM cells under different treatments. The concentration of Dox was fixed at 0.5 μM, and that of nanomaterial was used accordingly.

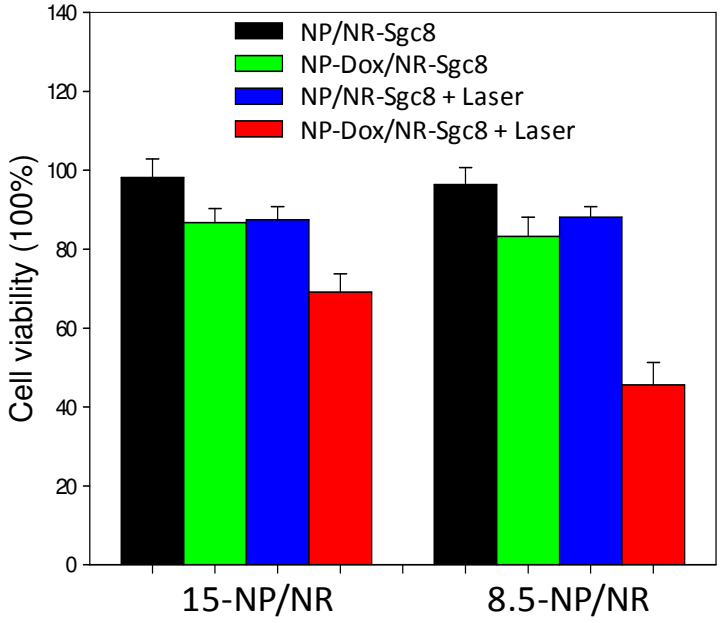

Figure S11. Cytotoxicity assay of CEM cells under different treatments. The concentration of Dox was fixed at 0.5 μM, and that of nanomaterials were used accordingly.

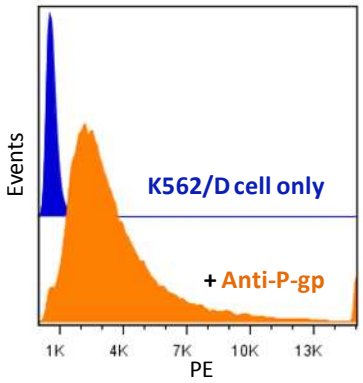

Figure S12. Flow cytometry assay of K562/D cells incubated with PE dye-labeled Mouse Anti-Human P-glycoprotein (Anti-P-gp).

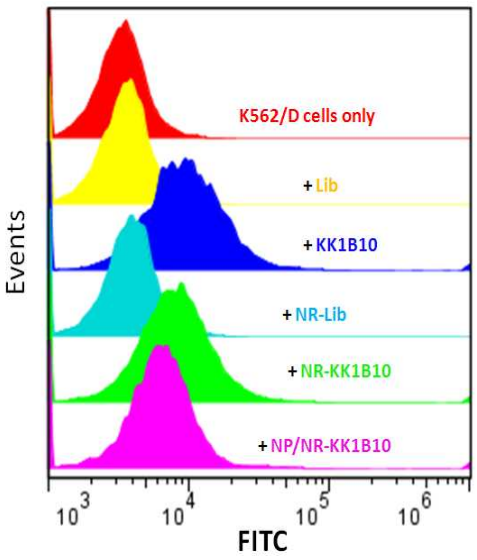

Figure S13. Flow cytometry assay of K562/D cells incubated with library sequence (Lib), KK1B10, NR-Lib, NR-KK1B10, and 15-NP/NR-KK1B10, respectively, at 4 ^{o}C for 30 min.

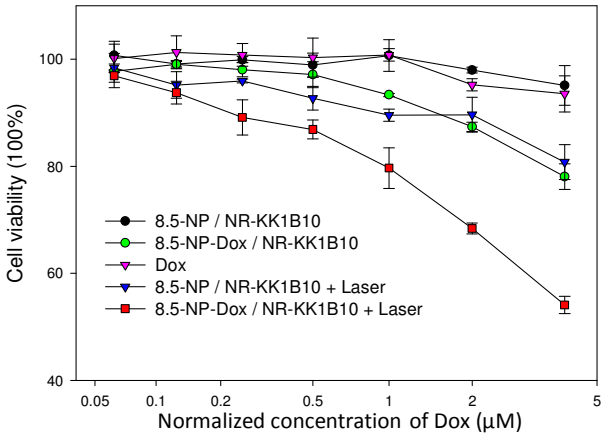

Figure S14. Cytotoxicity assay of K562/D cells under different treatments.

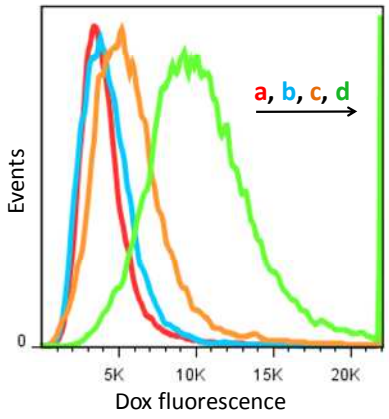

Figure S15. Flow cytometry assay to measure Dox fluorescence of K562/D cells under different treatments. The cells were incubated with 1×PBS (curve a), free Dox (5 μM, curve b), and 8.5-NP-Dox/NR-KK1B10s (equivalent of 5 μM Dox, curve c and curve d) at 37 ^{o}C for 2 h. After replacing the incubation solution with 1×PBS (the sample of curve c was irradiated with NIR laser for 10 min), the cells were kept at 37 ^{o}C for another 22 h.

References

1. Liu, J.; Lu, Y. Preparation of aptamer-linked gold nanoparticle purple aggregates for colorimetric sensing of analytes. *Nat. protoc.* **2006**, *1*, 246-252.
2. Jana, N. R.; Gearheart, L.; Murphy, C. J. Seeding growth for size control of 5-40 nm diameter gold nanoparticles. *Langmuir* **2001**, *17*, 6782-6786.
3. Yasun, E.; Gulbakan, B.; Ocsoy, I.; Yuan, Q.; Shukoor, M. I.; Li, C.; Tan, W. Enrichment and detection of rare proteins with aptamer-conjugated gold nanorods. *Anal. chem.* **2012**, *84*, 6008-6015.
4. Orendorff, C. J.; Murphy, C. J. Quantitation of metal content in the silver-assisted growth of gold nanorods. *J. Phys. Org. Chem.* **2006**, *110*, 3990-3994.
5. Xu, L.; Kuang, H.; Xu, C.; Ma, W.; Wang, L.; Kotov, N. A. Regiospecific plasmonic assemblies for in situ Raman spectroscopy in live cells. *J. Am. Chem. Soc.* **2012**, *134*, 1699-1709.